ACS APPLIED MATERIALS & INTERFACES
Research Article
www.acsami.org

MicroRNA-Responsive Cancer Cell Imaging and Therapy with Functionalized Gold Nanoprobe

Jintong Liu,[†] Lei Zhang,[†] Jianping Lei,[*] and Huangxian Ju

State Key Laboratory of Analytical Chemistry for Life Science, School of Chemistry and Chemical Engineering, Nanjing University, Nanjing 210093, People's Republic of China

Supporting Information

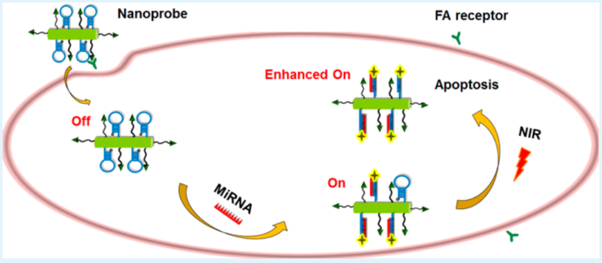

ABSTRACT: Integration of cancer cell imaging and therapy is critical to enhance the theranostic efficacy and prevent under- or overtreatment. Here, a multifunctional gold nanoprobe is designed for simultaneous miRNA-responsive fluorescence imaging and therapeutic monitoring of cancer. By assembling with folic acid as the targeted moiety and a dye-labeled molecular beacon (MB) as the recognition element and signal switch, the gold nanoprobe is folate receptor-targeted delivered into the cancer cells, and the fluorescence is lighted with the unfolding of MB by intracellular microRNA (miRNA), resulting in an efficient method for imaging and detecting nucleic acid. The average quantity of miRNA-21 is measured to be 1.68 pg in a single HeLa cell. Upon the near-infrared irradiation at 808 nm, the real-time monitoring and assessing of photothermal therapeutic efficacy is achieved from the further enhanced fluorescence of the dye-labeled MB, caused by the high photothermal transformation efficiency of the gold nanocarrier to unwind the remaining folded MB and depart the dye from the nanocarrier. The fluorescence monitoring is also feasible for applications in vivo. This work provides a simple but powerful protocol with great potential in cancer imaging, therapy, and therapeutic monitoring.

KEYWORDS: *nanoparticles, biosensors, microRNA, cell imaging, fluorescence*

INTRODUCTION

MicroRNAs (miRNAs), a class of small, noncoding, endogenous RNAs (approximately 19−25 nucleotides),[1,2] have essential functions in RNA silencing and post-transcriptional regulation of gene expression.[3−6] The growing evidence indicates that miRNAs have potential as diagnostic and prognostic biomarkers,[7,8] and their expression level is closely related to some major human diseases.[9] Therefore, quantitative detection and analysis of miRNAs expression are crucial to the early diagnosis, diseases cure, and the optimization of gene drugs correlated with miRNAs' regulation mechanism. To date, researchers have disclosed a number of methods,[10−12] including real-time polymerase chain reaction,[13−15] Northern blotting,[16,17] and DNA microarrays,[18−21] to face this challenge.[22] Significantly, benefiting from the rapid development of nanomaterials, several imaging methods were established for intracellular miRNA.[23−27] For example, a multifunctional SnO_2 nanoprobe conjugated with a recognition gene and a cell-targeting moiety is developed for specific detection of intracellular miRNA in our group.[28] Gold-nanobeacons are designed for simultaneous an endogenous miRNA-21 silencing and intracellular tracking of the silencing events.[29] But little research involved the integration of miRNAs-targeting imaging, real-time therapy and therapeutic monitoring of cancer cells, which is desirable and interesting in clinical diagnosis. To achieve this goal, a multifunctional nanocarrier is significantly needed.

Noble metal nanostructures have received a great deal of research interest in photothermal therapy, due to the good biocompatibility, strong absorption in near-infrared (NIR) region, and high photothermal conversion efficiency.[30,31] A series of metal nanocages,[32,33] hollow nanospheres,[34,35] nanorods,[36−38] and nanocomposites[39,40] are successfully applied as efficient photothermal reagents in therapy and imaging of cancers.[41] For example, the peptide functionalized gold nanorod probe was developed for visualization of matrix metalloprotease activity and photothermal therapy of cancer.[36] A multifunctional Fe_3O_4−Au core−shell nanoparticle was designed for constructing the magnetically targeted and NIR-responsive theranostic platform.[39] Unfortunately, the therapy in the previous methods lacks direct feedback signal for evaluating the therapeutic effectiveness. To address this issue, it is desirable to develop an integrated platform in a single nanocarrier for simultaneous cancer imaging, therapy, and in situ therapeutic monitoring.

In this work, using gold nanorod (AuNR) as the model of both nanocarrier and photothermal reagent inducing cell apoptosis, a functionalized gold nanoprobe was designed for in situ miRNA-responsive cancer cell imaging and therapeutical monitoring (Scheme 1). The multifunctional Au nanoprobe

Received: April 14, 2015
Accepted: August 14, 2015
Published: August 14, 2015

DOI: 10.1021/acsami.5b06206
ACS Appl. Mater. Interfaces 2015, 7, 19016−19023

Scheme 1. Schematic Illustration of in Situ Monitoring of Intracellular MiRNA and Theranostic Efficacy with Au Nanoprobe

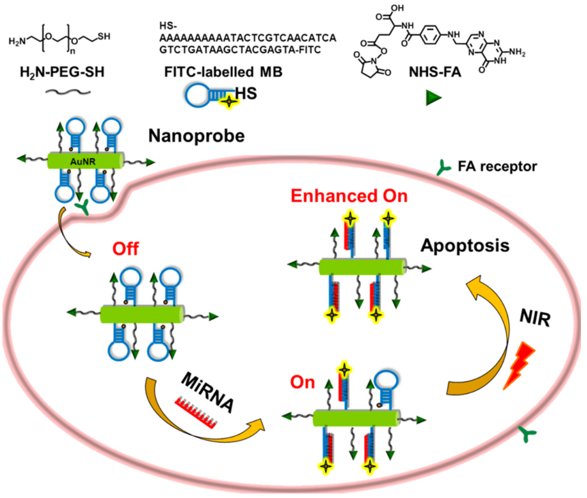

was assembled with fluorescein isothiocyanate (FITC)-labeled molecular beacon (MB) as the signal and recognition elements and folic acid (FA) as a target-specific moiety. The fluorescence of the probe was initially quenched via energy transfer from FITC to AuNR with transverse surface plasmon resonance (SPR) absorption, which is defined as the “off” state. Upon endocytosis, the fluorescence of the nanoprobe was recovered when the stem of MB was unfolded and the FITC dye was far from the AuNR, due to the specifical recognition of MB to the complementary sequence of intracellular miRNA-21, leading to a sensitive way for cancer cell-specific imaging and fluorescent detection of miRNA, therefore, the probe was in the “on” state. After NIR irradiation, cell apoptosis was induced by the heat from photothermal effect of AuNRs, and the fluorescence was further enhanced because the remaining folded MB could be unwinded into the single DNA in the condition of high temperature.[42] The further enhanced fluorescence signal defined as “enhanced on” state. Therefore, the fluorescence of the AuNR probe was a direct feedback of photothermal effect induced by the NIR irradiation and offered an efficient way for the monitoring the therapeutic efficiency in real time.

■ EXPERIMENTAL SECTION

Materials and Reagents. Hexadecyltrimethylammonium bromide (CTAB), chloroauric acid ($HAuCl_4 \cdot 4H_2O$), silver nitrate ($AgNO_3$), sodium borohydride ($NaBH_4$), and ascorbic acid were purchased from Sinopharm Chemical Reagent Co., Ltd. (China). Dicyclohexylcarbodiimide (DCC), *N*-hydroxysuccinimide (NHS), folic acid (FA), tris(2-carboxyethyl)phosphine(TCEP), and 3-(4,5-dimethylthiazol-2-yl)-2,5-diphenyltetrazolium bromide (MTT) were purchased from Sigma-Aldrich (St. Louis, MO). Lipofectamine 2000 (Lp2000) and serum-free medium (Opti-MEM) were obtained from Invitrogen Corporation (Grand Island, NY). LysoTracker Deep Red was purchased from Life Technologies (Grand Island, NY). HS-poly(ethylene glycol) (PEG)-NH$_2$ (M.W. 5000) was obtained from JenKem Technology Co. Ltd. (China). PE Annexin V apoptosis detection kit was purchased from BD Biosciences (San Jose, CA). Phosphate buffer saline (PBS, pH 7.4) contained 136.7 mM NaCl, 2.7 mM KCl, 8.72 mM Na_2HPO_4 and 1.41 mM KH_2PO_4. All other reagents were of analytical grade. All aqueous solutions were prepared using ultrapure water (≥18 MΩ, Milli-Q, Millipore). All RNA and DNA sequences were purchased from Shanghai GenePharma Co., Ltd. and Sangon Biological Engineering Technology Co., Ltd. (Shanghai, China), respectively. The DNA and RNA sequences included

MB: 5′-HS-AAAAAAAAAATACTCGTCAACATCAGTC-TGATAAGCTACG AGTA-FITC-3′;

MiRNA-21:5′-UAGCUUAUCAGACUGAUGUUGA-3′;

MiRNA-21 inhibitor: 5′-UCAACAUCAGUCUGAUAAGCUA-3′;

Single-base mismatched strand: 5′-UAGCUUAUCAGACUGAU-GUUCA-3′;

Two-base mismatched strand: 5′-UAGCUUAUCAGACAGAUGU-UCA-3′;

Three-base mismatched strand: 5′-UAACUUAUCAGACAGAUG-UUCA-3′.

The underlined letters represent the mismatched base.

Apparatus. The transmission electron microscopic (TEM) images were obtained on a JEM-2100 transmission electron microscope (JEOL Ltd., Japan). The UV−vis-NIR absorption spectra were obtained with a UV-3600 UV−vis-NIR spectrophotometer (Shimadzu Co., Kyoto, Japan). Zeta potential analysis was performed on a Zetasizer (Nano-Z, Malvern, UK). Raman spectra were recorded on a Laser Confocal Micro-Raman Spectroscopy (Via-Reflex, Britain). ^{1}HNMR spectra were recorded with a Bruker 500 MHz spectrometer. Fluorescence spectra were recorded on a RF-5301PC spectrofluorometer (Shimadzu, Japan). Laser scanning confocal microscopic (LSCM) images were gained on a TCS SP5 laser scanning confocal microscope (Leica, Germany). Flow cytometric analysis was performed on a Coulter FC-500 flow cytometer (Beckman Coulter, Pasadena, CA). MTT assay was performed on a microplate reader (680, Bio-Rad, Hercules, CA). Cell number was determined using a Petroff-Hausser cell counter (Radnor, PA). The size distribution of nanoparticles were evaluated by dynamic light scattering (DLS) using a Brookheaven BI9000AT system (Brookheaven Instruments Corporation, Holtsville, NY).

Synthesis of AuNRs. AuNRs were synthesized according to a typical seed-mediated growth method.[43] Briefly, gold seeds were prepared by adding freshly prepared ice-cold sodium borohydride (0.01 M, 3.6 mL) into a solution containing CTAB (0.2 M, 22.5 mL) and $HAuCl_4$ (0.01 M, 1.5 mL), with the addition of 22.5 mL ultrapure water and then stirring for 5 min. The resulting gold seed solution was left for 3 h. Meanwhile, growth solution was prepared by mixing CTAB (0.1 M, 240 mL), $HAuCl_4$ (0.01 M, 10.2 mL), $AgNO_3$ (0.01 M, 1.5 mL) and ascorbic acid (0.1 M, 1.62 mL). The AuNRs were finally obtained after the seed solution (1.2 mL) was gently added into the growth solution and left for 10 h.

Synthesis of MB Functionalized AuNRs. Before MB immobilization, 0.1 mM MB was incubated with 5 mM TCEP in 50 mM Tris/HCl (pH = 7.5) buffer for 1 h at room temperature to reduce S−S to SH group. Then the prepared AuNR solution was centrifuged at 8000 rpm at 25 °C for 5 min twice to remove excess CTAB and resuspended in 100 μL of ultrapure water. Then, 440 μL of tris-HCl buffer, 50 μL of 10 μM HS-PEG-NH$_2$, and 10 μL of 100 μM MB were added to the AuNR solution and incubated for 24 h at room temperature in the dark. The reaction solution was centrifuged at 8000 rpm for 5 min at 25 °C, and the obtained precipitate was washed twice to remove the unbound MB and HS-PEG-NH$_2$ as the supernatant. MB and HS-PEG-NH$_2$ could be immobilized onto AuNR surface via the Au−S bond. The resulting MB functionalized AuNRs were resuspended in ultrapure water for further experiments.

Preparation of Au Nanoprobe. NHS-FA was first synthesized for the coupling of HS-PEG-NH$_2$ on the surface of MB-functionalized AuNRs. Briefly, DCC (25 mg) and NHS (26 mg) were added to 5 mL of dimethylsufoxide (DMSO) containing FA (50 mg), and the reaction mixture was stirred overnight in the presence of triethylamine (30 μL) in the dark at room temperature. After filtration, the supernatant was concentrated to precipitate NHS-FA in anhydrous ether. NHS-FA as a yellow powder was obtained after the supernatant was washed with anhydrous ether and dried under vacuum.[44,45] Afterward, 1.0 mL of the MB-functionalized AuNR solution ($OD_{787\ nm}$ = 0.4) reacted with 20 μL of NHS-FA (0.1 M, in DMSO) in the condition of pH 11 for 15 min. The reaction solution was then centrifuged at 8000 rpm for 5 min to get the precipitates. The obtained

DOI: 10.1021/acsami.5b06206
ACS Appl. Mater. Interfaces 2015, 7, 19016−19023

precipitates were washed twice with PBS and finally resuspended in PBS as the AuNR probe for further use. The OD (optical density) value of the AuNR probe at 787 nm used in this work was 0.4 unless noted otherwise. Therefore, the concentration of the AuNR probe was 2.0 nM according to the OD value.[46]

Gel Electrophoresis Experiments. The 12% native polyacrylamide gel electrophoresis (PAGE) was performed by using the buffer of 1 × tris-borate-EDTA (TBE). Then, a 14 μL DNA sample was mixed with 3 μL 6 × loading buffer and 3 μL UltraPower dye to obtain the loading sample. The loading sample was placed for 3 min for the complete integration with DNA and applied onto the lane. The gel was run at 90 V for 90 min in 1 × TBE buffer and then scanned using a Molecular Imager Gel Doc XR (Bio-Rad, Hercules, CA).

Evaluation of the Amount of MB Loaded on AuNRs. The loading amount of MB on the AuNRs was determined by fluorescence measurement of the labeled dye. The fluorescence intensity of the supernatant, containing free MB removed from the particle, was converted to concentration of the corresponding MB with a standard linear calibration curve. The standard curve was obtained with known concentrations of MB. Finally, the average number of MB per particle was obtained by dividing the subtracted concentration of MB by the AuNR concentration.

In Vitro Detection of MiRNA-21. Twenty microliters (20 μL) of AuNR probe ($OD_{787\ nm} = 0.4$) was incubated with different amounts of miRNA-21 dissolved in diethy pyrocarbonate (DEPC) water (100 μL) at 37 °C for the designed times in DNA hybridization buffer (10 mM tris-HCl, pH = 7.5, and 50 mM NaCl), and the change of fluorescence intensity was measured. The fluorescence spectra were collected from 500 to 700 nm under an excitation at 490 nm.

Cell Culture. HeLa, A549 and HaCat cells were cultured in a flask in Dulbecco's modified Eagle's medium (DMEM, Gibco), and MCF-7 cell lines were cultured in Roswell Park Memorial Institute (RPMI)-1640 (Gibco), supplemented with 10% fetal calf serum (FCS, Gibco), penicillin (100 μg mL^{-1}), and streptomycin (100 μg mL^{-1}) at 37 °C in a humidified atmosphere containing 5% CO_2.[47] Cell numbers were determined with a Petroff-Hausser cell counter (Radnor, PA).

Cytotoxicity Evaluation. MTT assay was used to estimate the cytotoxicity of the nanoprobe, NIR irradiation, or both. Briefly, HeLa cells (100 μL, 1.0 × 10^5) were seeded in each well of 96-well plate containing 200 μL DMEM for 24 h. After rinsing with PBS, HeLa cells were incubated with 200 μL fresh culture media containing serial concentrations of AuNR probe for 3 h, exposed to NIR irradiation for different times, or both. As the control, the cells were incubated with 200 μL of culture medium without AuNR probe. Then, 20 μL of 5 mg mL^{-1} MTT solution in PBS was added to each well. After 4 h of incubation, the medium containing unreacted MTT was removed carefully, and 150 μL DMSO was added to each well to dissolve the produced blue formazan. After the cell plate was vibrated for 15 min, the absorbance at a wavelength of 560 nm was measured with a microplate reader. The cell viability (%) was then determined by $(A_{test}/A_{control}) \times 100$. The cytotoxicity of HaCat cells incubated with AuNR probe and then exposed to NIR for different times was evaluated by using the same procedure.

Colocalization Assay. For colocalization assay of the nanoprobe-transfected HeLa cells, HeLa cells were seeded into 35 mm confocal dishes (5 × 10^4) and incubated for 12 h at 37 °C. After incubated with AuNR probe for 3 h and washed with PBS, the cells were stained with 75 nM LysoTracker Deep Red for 15 min. The fluorescence of LysoTracker Deep Red was collected from 660 to 720 nm with a 633 nm laser.

Detecion of Intracellular MiRNA-21. MiRNA mimic is a kind of synthetic single-stranded RNA which can simulate the endogenous miRNA-21 of mature cells in a high-level expression. Therefore, the amount of intracellular miRNA can be measured with standard curve extrapolation using miRNA-21 mimic.[28] Different amounts of miRNA-21 mimic in Lp2000 were delivered into the living cells for 6 h. The quantity of miRNA-21 mimic internalized by the cells was calculated by the absorbance change of the media at 260 nm. The treated cells in 35 mm confocal dish were then incubated with fresh 500 μL Opti-MEM containing 20 μL AuNR probe for another 3 h, and then washed with PBS to perform confocal imaging analysis or collected and resuspended in binding buffer for flow cytometric analysis over FL1 channel. The inhibition experiment was carried out using the similar method by mixing with 500 nM anti-miRNA and the miRNA-21 mimic to treat the cells for 6 h.

Confocal Fluorescence Imaging After NIR Irradiation. HeLa cells were seeded in 35 mm confocal dishes at a density of 5 × 10^4 per dish and incubated for 12 h at 37 °C. The medium was then replaced with Opti-MEM containing 20 nM miRNA-21 mimic and incubated with the living cells for 6 h. The mimic-transfected cells were then treated with 20 μL of AuNR probe for another 3 h in Opti-MEM. After being irradiated for different times and gently washed with PBS, the fluorescence of cells was collected from 500 to 560 nm on a confocal laser scanning microscope with the excitation wavelength of 488 nm.

Flow Cytometric Assay to Monitor Cell Apoptosis. Briefly, HeLa cells (5.0 × 10^5) were seeded in a 6-well plate for 12 h containing 2 mL fresh DMEM in each well. These cells were sequentially treated with miRNA-21 mimic for 6 h, AuNR probe for 3 h and then NIR irradiation for different times. The treated cells were collected, stained with the mixture of 5.0 μL of Annexin V-PE and 5.0 μL of 7-amino-actinomycin D (7-AAD) for 15 min, and analyzed with flow cytometry over FL2 (Annexin V-PE) and FL3 (7-AAD).

Animal Experiments. The animal operations meet the requirements of institutional animal use and care approved by the Model Animal Research Center of Nanjing University. Specific pathogen-free female 5−6 weeks-age BALB/c nude mice were purchased from Shanghai Laboratory Animal Center, Chinese Academy of Sciences and bred in an axenic environment. The HeLa tumor model was established by subcutaneous injection of HeLa cells (1.0 × 10^6) into the selected position of the nude mice. During the experiment, mice were anesthetized with 2.5% isoflurane in oxygen at a flow rate of 1.5 L min^{-1}. For time-dependent in vivo imaging, one HeLa tumor-bearing mouse was intravenously injected with 100 μL AuNR probe via tail vein, and imaging was conducted on a Maestro EX in vivo Imaging System at 6, 12, 24, and 48 h postinjection. For the photothermal therapy (PTT), the HeLa-tumor-bearing mice were intravenously injected with 100 μL of 2.0 nM AuNR probe via tail vein and then treated with NIR irradiation for 40 min 24 h postinjection, for fluorescence imaging in vivo at different postirradiation times. To acquire the images, 2.5% isoflurane in oxygen was delivered at a flow rate of 1.5 L min^{-1} to anesthetize the mice in the PTT process. In vivo treatment outcome was studied by using a vernier to measure the tumor volume after treatment. The greatest longitudinal diameter (length) and the greatest transverse diameter (width) of each tumor were determined using a vernier caliper, and the tumor volume was calculated using length × width^2 × 0.5.[48] After the in vivo imaging, the excised organs and tumor tissue were obtained from the euthanized mice for ex vivo imaging.

■ RESULTS AND DISCUSSION

Synthesis and Characterization. Gold nanorods were first synthesized according to the seed-mediated growth method and were characterized by UV−vis spectra and TEM image (Figure 1A). The prepared AuNRs showed an aspect ratio of 3.8 with 11 nm in diameter and 42 nm in length, and a longitudinal SPR at 787 nm. To prepare AuNR probe, HS-poly(ethylene glycol) (PEG)-NH_2 was used to protect AuNRs from aggregation (Figure S1) and bind *N*-hydroxysuccinimide of FA (NHS-FA),[49] which was characterized by ^{1}HNMR spectra (Figure 1B). After functionalization with HS-PEG-NH_2 and MB, the characteristic absorption at 260 nm for DNA was observed in the UV−vis spectrum, while the binding of NHS-FA to the PEG produced a characteristic absorption peak at 280 and 320 nm assigned to FA.[50] The surface profile of AuNR did not change after the functionalization with PEG and MB (Figure S2). The loading amount of MB on the AuNR surface was determined to be 109 by using the fluorescence

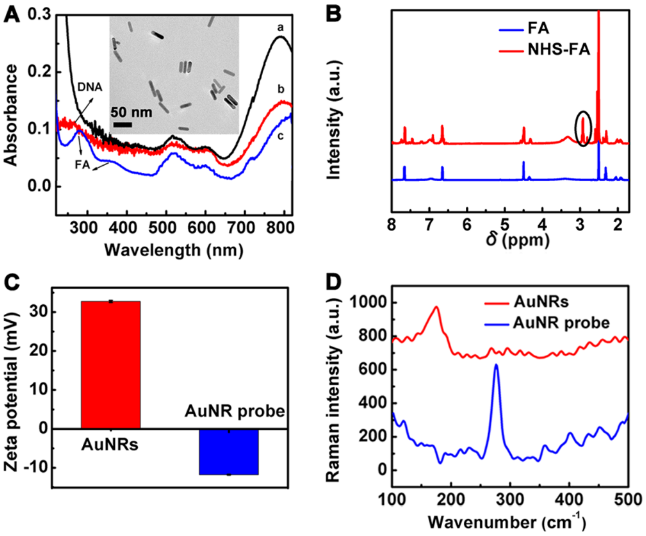

Figure 1. (A) UV−vis-NIR absorption spectra of (a) raw AuNRs, (b) HS-PEG-NH_2 and MB functionalized AuNRs, and (c) AuNR probe; (inset) TEM image of raw AuNRs. (B) ^{1}HNMR spectra of FA and NHS-FA. (C) Zeta potential and (D) Raman spectra of raw AuNRs and AuNR probe.

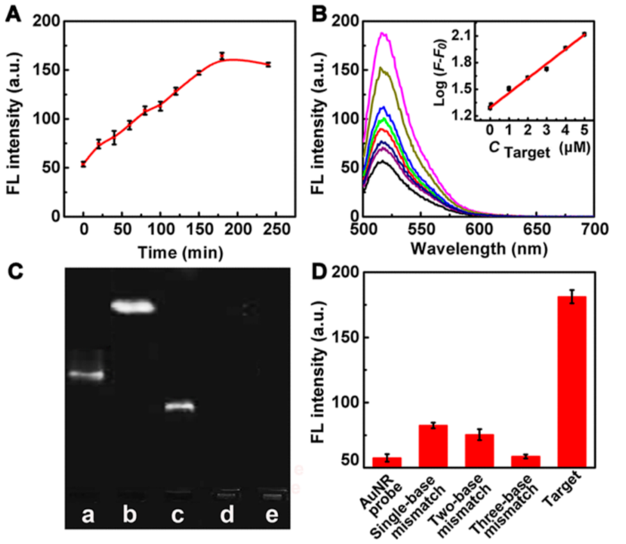

Figure 2. (A) Time-dependent fluorescence response of AuNR probe ($OD_{787\ nm}$ = 0.4, 20 μL) to miRNA-21 at the concentration of 5 μM at 517 nm. (B) Fluorescence response of AuNR probe to miRNA-21 at the concentrations of (bottom to top) 0, 0.001, 0.05, 1, 2, 3, 4, and 5 μM; (inset) calibration curve of logarithmic value of $F - F_0$ vs miRNA-21 concentration, where F_0 and F are the fluorescence intensity of AuNR probe without and with target miRNA after incubation for 180 min at 37 °C, respectively. (C) PAGE images of MB (a), miRNA-21 (b), MB + miRNA-21 (c), MB functionalized AuNRs (d) without and (e) with the addition of miRNA-21. (D) Fluorescence response of AuNR probe to the target miRNA (5 μM) and single/two/three-base mismatched miRNAs (50 μM).

measurement of the dye labeled to MB (Figure S3A), and the loading amount of FA was calculated to be 121 via UV−vis spectroscopy according to the similar procedure (Figure S3B). What's more, the Zeta potential of AuNR surface changed from postive to negative with the functionalization of MB (Figure 1C). From Raman spectra, the raw AuNRs showed an Au−Br peak at 181 cm^{-1} due to the presence of CTAB, which shifted to 262 cm^{-1} for the Au−S bond (Figure 1D). These results indicated that the Au nanoprobe was successfully synthesized for the following assays.

In Vitro Fluorescent Response to MiRNA-21. Because the emission of FITC overlapped with the transverse SPR absorption of AuNRs, the probe fluorescence was quenched via FRET (Figures S4 and S5). After incubating the mixture of the probe and the miRNA-21 in DEPC water at 37 °C, the fluorescence intensity was significantly enhanced at 517 nm, which was caused by the hybridization of the target with MB to unfold the hairpin, leading to the departure of FITC dye from the AuNRs. At the optimal reaction time of 180 min (Figure 2A), the fluorescence intensity linearly increased with the increasing concentration of miRNA-21 (Figure 2B). The hybridization reaction could be confirmed by the PAGE analysis (Figure 2C). Compared with individual MB and miRNA-21 (lanes a and b), the two-component mixture showed the band at shorter electrophoresis distance (lane c), indicating the successful formation of MB-target complex. No obvious band was observed when the MB was immobilized on AuNR with or without the addition of miRNA (lanes d and e), resulting from the big size of the AuNR, which hindered the migration. With the specific biorecognition, the prepared probe showed good selectivity to target miRNA against other base-mismatched miRNAs (Figure 2D). The signal change of perfectly complementary target was about 5.0 times of that for single-base mismatched sequence and the response to two/three-base mismatched strand was only 14.4 and 0.9% of that to miRNA-21, respectively.

FR-Mediated Endocytosis of Au Nanoprobe. Before intracellular usage, the cytotoxicity of AuNR probe was exactly evaluated with the MTT assay. After HeLa cells were treated with the probe from 0 to 50 μL for 3 h, the cells still exhibited a high viability of ∼96.1% (Figure 3A), suggesting that AuNR probe possessed good biocompatibility. The 95.9% viability of HeLa cells after treated with NIR irradiation for different times indicated the low cytotoxicity of NIR irradiation in the absence of AuNR probe (Figure 3B). Compared with HaCat normal cells with negative expresstion of FA receptor (FR), the AuNR probe transfected HeLa cells showed obvious cytotoxicity under the NIR irradiation for different times (Figure 3C), which could be attributed to the FR-targeted endocytosis of the Au nanoprobe. Meanwhile, both the HeLa cells and HaCat normal cells transfected by the nanoprobe without folic acid showed high viability under the NIR irradiation (Figure S6). In the absence of NIR irradiation, the cell viability of both HeLa and HaCat cells could still maintain about 90% after being incubated with Au nanoprobe for 48 h (Figure S7).

The targeted delivery of the AuNR probe into cancer cells by the recognition to FA receptor overexpressed on cell membrane was further comfirmed by confocal fluorescence imaging experiments. The weak fluorescence of FITC could be observed in MCF-7 and HeLa cells with high-expression of FA receptor, while no change was observed in A549 cells with negative FA receptor (Figure S8). For subcellular localization of the probe, the confocal microscopic images were taken, which showed that the spot of AuNR probe overlapped with the lysosomal tracker, LysoTracker Deep Red (Figure S9), indicating the AuNR probe could be delivered into lysosome after internalization. By the leakage from lysosome due to the damage in lysosomal membrane integrity, AuNR probe was then released to the cytoplasm and delivered to mitochondria.[30]

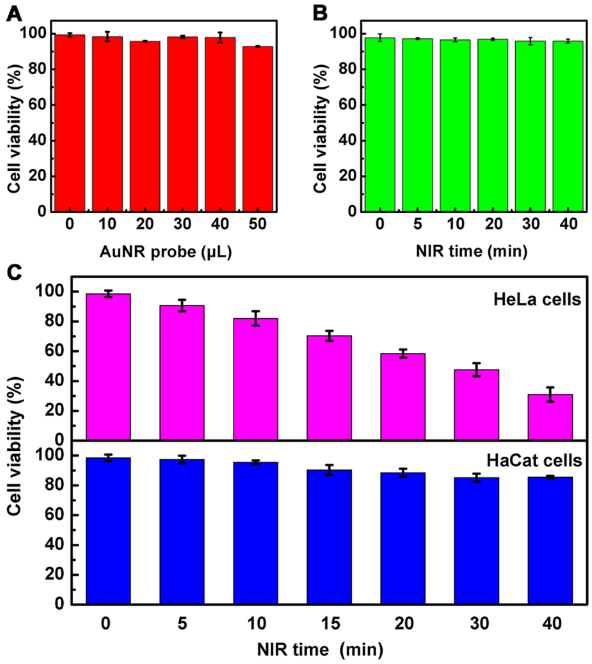

Figure 3. Viability of HeLa cells after (A) incubation with different amounts of AuNR probe for 3 h, (B) NIR irradiation at 3 W cm^{-2} for different times, and (C) incubation with AuNR probe (20 μL) for 3 h and then with NIR irradiation for different times compared with HaCat normal cells.

Imaging and Detection of Intracellular MiRNA. For quantitative detection of miRNA in living cells, HeLa cells were first transfected with different amounts of miRNA-21 mimic for 6 h, and then incubated with AuNR probe for 3 h. As shown in Figure 4B, the confocal microscopic images showed brighter fluorescence with the increasing amount of miRNA-21 mimic transfected into the cells. As a control, the miRNA-21 inhibitor (anti-miRNA) pretreated HeLa cells displayed little fluorescence (Figure 4A), although the addition of the same amount of miRNA-21 mimic, as in Figure 4B, demonstrated the specific response of intracellular miRNA-21. The plot of fluorescence intensity versus the amount of miRNA-21 mimics transfected into the cell showed a good linear relationship, $I = 1.12\ C_{\text{miRNA mimic}} + 1.88$, with a related coefficient of 0.998 (Figure 5A). The average quantity of miRNA-21 in a single HeLa cell could be calculated as 1.68 pg from the above linear regression equation, which was in good aggrement of the relative report.[28] To further confirm the feasibility of the proposed method, we conducted flow cytometric analysis to detect the miRNA. The obtained linear regression equation was $I = 1.87\ C_{\text{miRNA mimic}} + 3.05$ ($R^2 = 0.998$, Figure 5B), and the average quantity of miRNA-21 was 1.62 pg in single HeLa cell. It was 3.5% relative deviation between the confocal and flow cytometric methods, demonstrating good validation of the proposed nanoprobe. Thus, the designed Au nanoprobe could be used for in situ imaging and detection of intracellular miRNA.

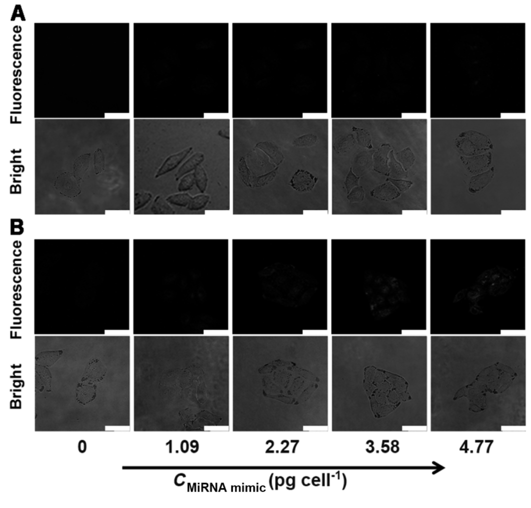

Figure 4. Confocal fluorescence and bright-field images of HeLa cells transfected with different amounts of miRNA-21 pretreated (A) with and (B) without anti-miRNA and then incubated with 20 μL AuNR probe for 3 h at 37 °C. Scale bars: 50 μm.

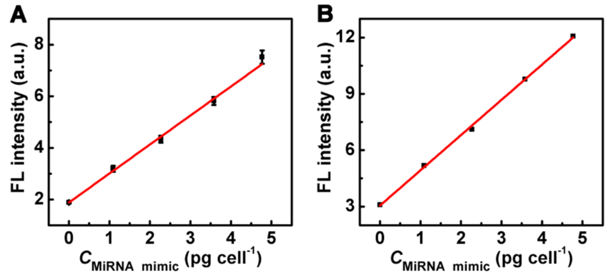

Figure 5. Plots of mean FL intensities from (A) confocal imaging and (B) flow cytometric analysis vs the quantity of intracellular miRNA-21.

Monitoring of Therapeutic Efficacy. Although the fluorescence was lighted with the response of intracellular miRNA, the enhanced fluorescence after NIR irradiation further made it possible to directly assess therapeutic efficacy using the Au nanoprobe. To verify this capability, we tracked the confocal fluorescence imaging of AuNR probe transfected HeLa cells under NIR irradiation for different times in the response of intracellular miRNA. The fluorescence was observed to become brighter with the deepened apoptosis degree (Figure 6A), which was proved by the flow cytometric analysis. The mean fluorescence intensity of the treated HeLa cells obviously increased during the NIR irradiation, and the cell apoptosis was aggravated with the assays of Annexin V-PE/7-AAD kit (Figure 6B,C). This phenomenon should be explained as that the remaining locked MB on the AuNR was not stable with the increasing temperature caused by the photothermal effect of AuNRs[51] and unfolded into the single-strand DNA, thus resulting in the FITC departure from AuNRs and then a further enhanced fluorescence. As control, the fluorescence intensity increase induced from only NIR irradiation was proved both in vitro and in living cells (Figure S10 and Figure 7). Therefore, the probe fluorescence greatly depended on the cell apoptosis induced by AuNRs-mediated therapy. In vitro fluorescence measurement demonstrated the similar signal changes of the designed Au nanoprobe after sequential responding by miRNA-21 and treatment with NIR irradiation (Figure 7). These results indicated that the functionalized Au nanoprobe not only had the potential for in situ detection of intracellular miRNA but also could be used for real-time monitoring the therapeutic efficacy of targeted-cancer cell, providing a novel tool to evaluate the therapeutic responses.

Monitoring of Therapeutic Efficacy in Living Mouse. The nanoprobe was applied to monitor the therapeutic effect in

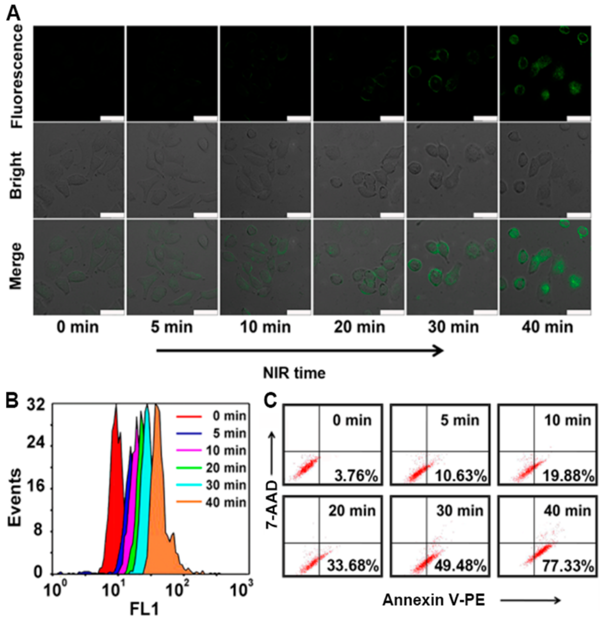

Figure 6. (A) Confocal fluorescence and bright-field images, (B) flow cytometric detection and (C) flow cytometric analysis using apoptosis kit with the dual fluorescence of Annexin V-PE/7-AAD of HeLa cells sequentially treated with 20 nM miRNA-21 mimic for 6 h, AuNR probe (20 μL) for 3 h, and NIR irradiation for different times. Scale bars: 50 μm.

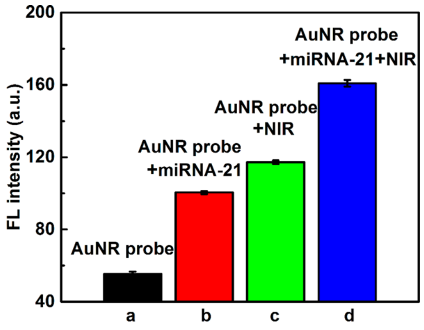

Figure 7. Fluorescence intensities of (a) AuNR probe ($OD_{787\ nm}$ = 0.4), (b) AuNR probe incubated with miRNA-21 at 37 °C for 180 min, AuNR probe incubated (c) without and (d) with miRNA-21 at 37 °C for 180 min and then NIR irradiation for 10 min.

living mice via real-time NIR irradiation. Usually, the autofluorescence of melanin and hemoglobin in vivo has a great effect on the fluorescence of FITC at 500−550 nm. However, the autofluorescence can be greatly reduced when excited at the NIR wavelength for cyanine-5.5 (Cy5.5). Therefore, FITC dye was replaced with Cy5.5 to label MB in this experiment. The HeLa tumor was subcutaneously implanted on the flank of the nude mice. The tumor-bearing mice were then intravenously injected with AuNR probe for time-dependent imaging. By the determination of DLS and Zeta potential, the AuNR probe showed well stability in blood for 72 h, due to the presence of PEG components (Figure S11).[52,53] The accumulation of the probe was observed to be highly efficient in the tumor at 24 h postinjection (Figure 8A). Then, the mice were irradiated with an 808 nm NIR laser for 40 min to perform the photothermal therapy. The efficacy of AuNR-mediated therapy could be assessed by monitoring the fluorescence change using in vivo imaging, which showed that the fluorescence increased gradually after 6, 12, and 24 h postirradiation (Figure 8B), while no obvious change was displayed from the mouse 24 h postinjection of the AuNR probe in the absence of irradiation. The evaluation of excised tissues further demonstrated that the strong fluorescence occurred in the cancer tissue compared with the other organs including heart and lung (Figure 8C), indicating that the MB was unfolded by the photothermal effect. Meanwhile, the fluorescence in the liver was ascribed to the low accumulation of AuNR,[54] and the fluorescence in intestine originated from the food for specially feeding the nude mice. The therapeutic efficacy was also reflected by the tumor volume measurement for 15 days after treatment (Figure 8D). Both the nanoprobe- and NIR irradiation-treated mice showed significantly reduced tumor volume, while the ones injected with the AuNR probe in the absence of irradiation had rapidly promoted volume. In addition, no noticeable abnormality was observed in the H&E stained organ slices from untreated healthy mice and treated mice with the probe injection taken 15 days after photothermal therapy (Figure S12), demonstrating the negligible side effects of Au nanoprobe in vivo. Overall, the designed Au nanoprobe has the capability of monitoring the therapeutic efficiency with fluorescence signal in vivo.

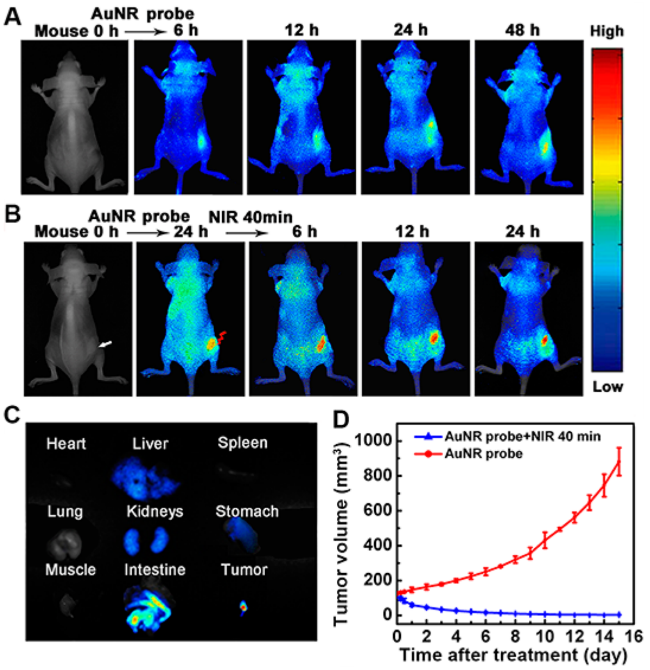

Figure 8. Time-dependent in vivo fluorescence images of subcutaneous HeLa tumor-bearing mouse after injected with AuNR probe (A) without and (B) with laser irradiation for 40 min. (C) Ex vivo fluorescence image of organs and cancer tissue 24 h postirradiation from HeLa tumor-bearing mouse treated with 24 h postinjection of AuNR probe. (D) Change of tumor volume after treatment with 24-h postinjection of AuNR probe and then with or without NIR irradiation for 40 min.

CONCLUSION

This work designs a multifunctional Au nanoprobe for simultaneous miRNA-responsive cell imaging and therapeutic efficacy monitoring. The nanoprobe possesses good solubility, good biocompatibility, targeted delivery, specificity to intracellular miRNA, and high photothermal conversion efficiency. After FA receptor-mediated endocytosis, the quenched probe fluorescence is recovered due to the unfolding of MB recognized by intracellular miRNA for cancer-cell imaging, leading to an in situ quantitative method. Furthermore, the enhanced fluorescence upon the NIR irradiation can be used as a direct tool to evaluate the photothermal therapeutic efficacy with AuNRs, which is also successfully applied in vivo. The proposed strategy not only develops a promising miRNA quantification and imaging method but also provides an integrated platform with the functions of cancer detection, therapy, and therapeutic monitoring for biomedical research and clinical diagnosis.

ASSOCIATED CONTENT

Supporting Information

The Supporting Information is available free of charge on the ACS Publications website at DOI: 10.1021/acsami.5b06206.

> Absorption spectrum of HS-PEG-NH_2 functionalized AuNRs; TEM image of the functionalized nanoprobe; amounts of MB and FA loaded on the nanocarrier; quenching effect of gold nanocarrier on FITC; cytotoxicity of nanoprobe without FA to HeLa and HaCat cells; cytotoxicity of Au nanoprobe to HeLa and HaCat cells; FR-mediated endocytosis of the Au nanoprobe; subcellular localization of the nanoprobe; stability of AuNR probe in blood; in vivo biocompatibility of the nanoprobe. (PDF)

AUTHOR INFORMATION

Corresponding Author

* Phone/Fax: +86-25-83593593. E-mail: jpl@nju.edu.cn.

Author Contributions

[†]These authors contributed equally. All authors have given approval to the final version of the manuscript.

Notes

The authors declare no competing financial interest.

ACKNOWLEDGMENTS

We gratefully acknowledge the National Natural Science Foundation of China (21375060, 21135002, 21121091) and Doctoral Program of Higher Education of China in Priority Development Areas (20130091130005).

REFERENCES

(1) Ambros, V. The Functions of Animal MicroRNAs. *Nature* **2004**, *431*, 350−355.

(2) Cissell, K. A.; Shrestha, S.; Deo, S. K. MicroRNA Detection: Challenges for the Analytical Chemist. *Anal. Chem.* **2007**, *79*, 4754−4761.

(3) He, L.; Hannon, G. J. MicroRNAs: Small RNAs with a Big Role in Gene Regulation. *Nat. Rev. Genet.* **2004**, *5*, 522−531.

(4) Lu, J.; Getz, G.; Miska, E. A.; Alvarez-Saavedra, E.; Lamb, J.; Peck, D.; Sweet-Cordero, A.; Ebert, B. L.; Mak, R. H.; Ferrando, A. A.; Downing, J. R.; Jacks, T.; Horvitz, H. R.; Golub, T. R. MicroRNA Expression Profiles Classify Human Cancers. *Nature* **2005**, *435*, 834−838.

(5) Carrington, J. C.; Ambros, V. Role of MicroRNAs in Plant and Animal Development. *Science* **2003**, *301*, 336−338.

(6) Brennecke, J.; Hipfner, D. R.; Stark, A.; Russell, R. B.; Cohen, S. M. Bantam Encodes a Developmentally Regulated MicroRNA that Controls Cell Proliferation and Regulates the Proapoptotic Gene Hid in Drosophila. *Cell* **2003**, *113*, 25−36.

(7) Ng, E. K. O.; Chong, W. W. S.; Jin, H.; Lam, E. K. Y.; Shin, V. Y.; Yu, J.; Poon, T. C. W.; Ng, S. S. M.; Sung, J. J. Y. Differential Expression of MicroRNAs in Plasma of Patients with Colorectal Cancer: A Potential Marker for Colorectal Cancer Screening. *Gut* **2009**, *58*, 1375−1381.

(8) Bianchi, F.; Nicassio, F.; Marzi, M.; Belloni, E.; Dall'Olio, V.; Bernard, L.; Pelosi, G.; Maisonneuve, P.; Veronesi, G.; Di Fiore, P. P. A Serum Circulating MiRNA Diagnostic Test to Identify Asymptomatic High-Risk Individuals with Early Stage Lung Cancer. *Embo Mol. Med.* **2011**, *3*, 495−503.

(9) Keller, A.; Leidinger, P.; Bauer, A.; Elsharawy, A.; Haas, J.; Backes, C.; Wendschlag, A.; Giese, N.; Tjaden, C.; Ott, K. Toward the Blood-Borne Mirnome of Human Diseases. *Nat. Methods* **2011**, *8*, 841−843.

(10) Bi, S.; Zhang, J. L.; Hao, S. Y.; Ding, C. F.; Zhang, S. S. Exponential Amplification for Chemiluminescence Resonance Energy Transfer Detection of MicroRNA in Real Samples Based on a Cross-Catalyst Strand-Displacement Network. *Anal. Chem.* **2011**, *83*, 3696−3702.

(11) Liu, H. Y.; Li, L.; Wang, Q.; Duan, L. L.; Tang, B. Graphene Fluorescence Switch-Based Cooperative Amplification: A Sensitive and Accurate Method to Detection MicroRNA. *Anal. Chem.* **2014**, *86*, 5487−5493.

(12) Dong, H. F.; Lei, J. P.; Ding, L.; Wen, Y. Q.; Ju, H. X.; Zhang, X. J. MicroRNA: Function, Detection, and Bioanalysis. *Chem. Rev.* **2013**, *113*, 6207−6233.

(13) Baker, M. MicroRNA Profiling: Separating Signal from Noise. *Nat. Methods* **2010**, *7*, 687−692.

(14) Wark, A. W.; Lee, H. J.; Corn, R. M. Multiplexed Detection Methods for Profiling MicroRNA Expression in Biological Samples. *Angew. Chem., Int. Ed.* **2008**, *47*, 644−652.

(15) Li, J.; Yao, B.; Huang, H.; Wang, Z.; Sun, C. H.; Fan, Y.; Chang, Q.; Li, S. L.; Wang, X.; Xi, J. Z. Real-Time Polymerase Chain Reaction MicroRNA Detection Based on Enzymatic Stem-Loop Probes Ligation. *Anal. Chem.* **2009**, *81*, 5446−5451.

(16) Pall, G. S.; Codony-Servat, C.; Byrne, J.; Ritchie, L.; Hamilton, A. Carbodiimide-Mediated Cross-Linking of RNA to Nylon Membranes Improves the Detection of SiRNA, MiRNA and PiRNA by Northern Blot. *Nucleic Acids Res.* **2007**, *35*, e60.

(17) Varallyay, E.; Burgyan, J.; Havelda, Z. MicroRNA Detection by Northern Blotting Using Locked Nucleic Acid Probes. *Nat. Protoc.* **2008**, *3*, 190−196.

(18) Chapin, S. C.; Appleyard, D. C.; Pregibon, D. C.; Doyle, P. S. Rapid MicroRNA Profiling on Encoded Gel Microparticles. *Angew. Chem., Int. Ed.* **2011**, *50*, 2289−2293.

(19) Duan, D. M.; Zheng, K. X.; Shen, Y.; Cao, R.; Jiang, L.; Lu, Z. X.; Yan, X. Y.; Li, J. Label-Free High-Throughput MicroRNA Expression Profiling from Total RNA. *Nucleic Acids Res.* **2011**, *39*, e154.

(20) Shen, Y.; Zheng, K. X.; Duan, D. M.; Jiang, L.; Li, J. Label-Free MicroRNA Profiling Not Biased by 3′End 2′-*O*-Methylation. *Anal. Chem.* **2012**, *84*, 6361−6365.

(21) Jinek, M.; Doudna, J. A. A Three-Dimensional View of the Molecular Machinery of RNA Interference. *Nature* **2009**, *457*, 405−412.

(22) Dangwal, S.; Bang, C.; Thum, T. Novel Techniques and Targets in Cardiovascular MicroRNA Research. *Cardiovasc. Res.* **2012**, *93*, 545−554.

(23) Dong, H. F.; Ding, L.; Yan, F.; Ji, H. X.; Ju, H. X. The Use of Polyethylenimine-Grafted Graphene Nanoribbon for Cellular Delivery of Locked Nucleic Acid Modified Molecular Beacon for Recognition of MicroRNA. *Biomaterials* **2011**, *32*, 3875−3882.

(24) Geng, Y.; Lin, D. J.; Shao, L. J.; Yan, F.; Ju, H. X. Cellular Delivery of Quantum Dot-Bound Hybridization Probe for Detection of Intracellular Pre-MicroRNA Using Chitosan/Poly(c-Glutamic Acid) Complex as a Carrier. *PLoS One* **2013**, *8*, e65540.

(25) Raj, A.; van den Bogaard, P.; Rifkin, S. A.; van Oudenaarden, A.; Tyagi, S. Imaging Individual mRNA Molecules Using Multiple Singly Labeled Probes. *Nat. Methods* **2008**, *5*, 877−879.

(26) Politz, J. C. R.; Zhang, F.; Pederson, T. MicroRNA-206 Colocalizes with Ribosome-Rich Regions in both the Nucleolus and

Cytoplasm of Rat Myogenic Cells. *Proc. Natl. Acad. Sci. U. S. A.* **2006**, *103*, 18957−18962.

(27) Liao, X. J.; Wang, Q. B.; Ju, H. X. Simultaneous Sensing of Intracellular MicroRNAs with a Multifunctionalized Carbon Nitride Nanosheet Probe. *Chem. Commun.* **2014**, *50*, 13604−13607.

(28) Dong, H. F.; Lei, J. P.; Ju, H. X.; Zhi, F.; Wang, H.; Guo, W.; Zhu, Z.; Yan, F. Target-Cell-Specific Delivery, Imaging, and Detection of Intracellular MicroRNA with a Multifunctional SnO_2 Nanoprobe. *Angew. Chem., Int. Ed.* **2012**, *51*, 4607−4612.

(29) Conde, J.; Rosa, J.; de la Fuente, J. M.; Baptista, P. V. Gold-Nanobeacons for Simultaneous Gene Specific Silencing and Intracellular Tracking of the Silencing Events. *Biomaterials* **2013**, *34*, 2516−2523.

(30) Huff, T. B.; Tong, L.; Zhao, Y.; Hansen, M. N.; Cheng, J. X.; Wei, A. Hyperthermic Effects of Gold Nanorods on Tumor Cells. *Nanomedicine* **2007**, *2*, 125−132.

(31) Yang, L.; Tseng, Y. T.; Suo, G.; Chen, L.; Yu, J.; Chiu, W. J.; Huang, C. C.; Lin, C. H. Photothermal Therapeutic Response of Cancer Cells to Aptamer−Gold Nanoparticle-Hybridized Graphene Oxide under NIR Illumination. *ACS Appl. Mater. Interfaces* **2015**, *7*, 5097−5106.

(32) Wang, Z. Z.; Chen, Z. W.; Liu, Z.; Shi, P.; Dong, K.; Ju, E. G.; Ren, J. S.; Qu, X. G. A Multi-Stimuli Responsive Gold Nanocage-Hyaluronic Platform for Targeted Photothermal and Chemotherapy. *Biomaterials* **2014**, *35*, 9678−9688.

(33) Xia, Y. N.; Li, W. Y.; Cobley, C. M.; Chen, J. Y.; Xia, X. H.; Zhang, Q.; Yang, M. X.; Cho, E. C.; Brown, P. K. Gold Nanocages: From Synthesis to Theranostic Applications. *Acc. Chem. Res.* **2011**, *44*, 914−924.

(34) You, J.; Zhang, G. D.; Li, C. Exceptionally High Payload of Doxorubicin in Hollow Gold Nanospheres for Near-Infrared Light Triggered Drug Release. *ACS Nano* **2010**, *4*, 1033−1041.

(35) Lu, W.; Zhang, G. D.; Zhang, R.; Flores, L. G.; Huang, Q.; Gelovani, J. G.; Li, C. Tumor Site-Specific Silencing of NF-κB p65 by Targeted Hollow Gold Nanosphere-Mediated Photothermal Transfection. *Cancer Res.* **2010**, *70*, 3177−3188.

(36) Yi, D. K.; Sun, I.-C.; Ryu, J. H.; Koo, H.; Park, C. W.; Youn, I.-C.; Choi, K.; Kwon, I. C.; Kim, K.; Ahn, C.-H. Matrix Metalloproteinase Sensitive Gold Nanorod for Simultaneous Bioimaging and Photothermal Therapy of Cancer. *Bioconjugate Chem.* **2010**, *21*, 2173−2177.

(37) Huang, X. H.; Neretina, S.; El-Sayed, M. A. Gold Nanorods: From Synthesis and Properties to Biological and Biomedical Applications. *Adv. Mater.* **2009**, *21*, 4880−4910.

(38) Liu, X. S.; Huang, N.; Li, H.; Wang, H. B.; Jin, Q.; Ji, J. Multidentate Polyethylene Glycol Modified Gold Nanorods for in Vivo Near-Infrared Photothermal Cancer Therapy. *ACS Appl. Mater. Interfaces* **2014**, *6*, 5657−5668.

(39) Li, W. P.; Liao, P. Y.; Su, C. H.; Yeh, C. S. Formation of Oligonucleotide-Gated Silica Shell-Coated Fe_3O_4-Au Core-Shell Nanotrisoctahedra for Magnetically Targeted and Near-Infrared Light-Responsive Theranostic Platform. *J. Am. Chem. Soc.* **2014**, *136*, 10062−10075.

(40) Wang, L. Y.; Bai, J. W.; Li, Y. J.; Huang, Y. Multifunctional Nanoparticles Displaying Magnetization and Near-IR Absorption. *Angew. Chem., Int. Ed.* **2008**, *47*, 2439−2442.

(41) Shanmugam, V.; Selvakumar, S.; Yeh, C. S. Near-Infrared Light-Responsive Nanomaterials in Cancer Therapeutics. *Chem. Soc. Rev.* **2014**, *43*, 6254−6287.

(42) Ke, G. L.; Wang, C. M.; Ge, Y.; Zheng, N. F.; Zhu, Z.; Yang, C. Y. J. L-DNA Molecular Beacon: A Safe, Stable, and Accurate Intracellular Nano-thermometer for Temperature Sensing in Living Cells. *J. Am. Chem. Soc.* **2012**, *134*, 18908−18911.

(43) Huang, X. H.; El-Sayed, I. H.; Qian, W.; El-Sayed, M. A. Cancer Cell Imaging and Photothermal Therapy in the Near-Infrared Region by Using Gold Nanorods. *J. Am. Chem. Soc.* **2006**, *128*, 2115−2120.

(44) Singh, P.; Gupta, U.; Asthana, A.; Jain, N. K. Folate and Folate-PEG-PAMAM Dendrimers: Synthesis, Characterization, and Targeted Anticancer Drug Delivery Potential in Tumor Bearing Mice. *Bioconjugate Chem.* **2008**, *19*, 2239−2252.

(45) Lee, R. J.; Low, P. S. Delivery of Liposomes into Cultured KB Cells via Folate Receptor-mediated Endocytosis. *J. Biol. Chem.* **1994**, *269*, 3198−3204.

(46) Orendorff, C. J.; Murphy, C. J. Quantitation of Metal Content in the Silver-Assisted Growth of Gold Nanorods. *J. Phys. Chem. B* **2006**, *110*, 3990−3994.

(47) Ke, G. L.; Zhu, Z.; Wang, W.; Zou, Y.; Guan, Z. C.; Jia, S. S.; Zhang, H. M.; Wu, X. M.; Yang, C. Y. J. A Cell-Surface-Anchored Ratiometric Fluorescent Probe for Extracellular pH Sensing. *ACS Appl. Mater. Interfaces* **2014**, *6*, 15329−15334.

(48) Euhus, D. M.; Hudd, C.; LaRegina, M. C.; Johnson, F. E. Tumor Measurement in the Nude Mouse. *J. Surg. Oncol.* **1986**, *31*, 229−234.

(49) Liao, H. W.; Hafner, J. H. Gold Nanorod Bioconjugates. *Chem. Mater.* **2005**, *17*, 4636−4641.

(50) Jin, H.; Yang, P. H.; Cai, J. Y.; Wang, J. H.; Liu, M. Photothermal Effects of Folate-Conjugated Au Nanorods on HepG2 Cells. *Appl. Microbiol. Biotechnol.* **2012**, *94*, 1199−1208.

(51) Huang, X.; Jain, P. K.; El-Sayed, I. H.; El-Sayed, M. A. Determination of the Minimum Temperature Required for Selective Photothermal Destruction of Cancer Cells Using Immunotargeted Gold Nanoparticles. *Photochem. Photobiol.* **2006**, *82*, 412−417.

(52) Poon, Z.; Lee, J. B.; Morton, S. W.; Hammond, P. T. Controlling in Vivo Stability and Biodistribution in Electrostatically Assembled Nanoparticles for Systemic Delivery. *Nano Lett.* **2011**, *11*, 2096−2103.

(53) Wang, R. R.; Xiao, R. Z.; Zeng, Z. W.; Xu, L. L.; Wang, J. J. Application of Poly(Ethylene Glycol)−Distearoylphosphatidylethanolamine (PEG-DSPE) Block Copolymers and Their Derivatives as Nanomaterials in Drug Delivery. *Int. J. Nanomed.* **2012**, *7*, 4185−4198.

(54) Jokerst, J. V.; Cole, A. J.; Van de Sompel, D.; Gambhir, S. S. Gold Nanorods for Ovarian Cancer Detection with Photoacoustic Imaging and Resection Guidance via Raman Imaging in Living Mice. *ACS Nano* **2012**, *6*, 10366−10377.